Geodetic Study of the Interseismic Coupling in the Central Andes and Post-seismic Deformation Following the March 11, 2011 M9.0 Tohoku-Oki Earthquake

Francisco Ortega[1] (ortega@caltech.edu), Mark Simons[1], Jeff Genrich[1], Susan Owen[6], Angelyn Moore[6], John Galetzka[1], Diana Comte[2], Bianca Glass[3], Carlos Leiva[3], Gabriel González[4], Edmundo Norabuena[5]

(1) Seismological Laboratory, California Institute of Technology, Pasadena, California 91125, USA. (2) Universidad de Chile, Santiago, Chile. (3) Universidad de Tarapacá, Arica, Chile. (4) Universidad Católica del Norte, Antofagasta, Chile. (5) Instituto Geofísico del Perú, Lima, Perú. (6) Jet Propulsion Laboratory, Pasadena, CA 91109, USA.

Introduction

We aim to understand the spatial variations of fault zone rheology in subduction zone megathrusts during the different stages of the seismic cycle. Our general approach uses geodetic measurements of crustal deformation at the different stages of the seismic cycle to infer kinematic models of inter-seismic coupling, co-seismic slip and post-seismic creep with the eventual goal of understanding the relationships between these different types of fault slip behavior (ex: apparent coupling v/s rupture zone of big earthquakes), as well as the implications for earthquake and tsunami hazard.

We approach the problem from a Bayesian perspective, in which we seek en ensemble of all the possible slip distributions allowed by the parameterization of the physical model instead of looking for a single optimum model. The main advantages of the Bayesian approach are that we are not required to use any form of regularization in our slip models other than the imposed by the parameterization and that we get accurate representations of model parameter uncertainties in the form of a probability density functions.

We apply this methodology to an interseismic coupling model of the Central Andes Megathrust and postseismic models for the Japan Trench subduction zone. All models are constrained by observations from dense regional continuous GPS networks.

Continuous GPS Data Processing

Raw data from cGPS sites is processed using the softwares GAMIT (Central Andes) and GIPSY (Japan) to produce positional time series for each site on the GPS network. The positional time series contain a secular motion due to interseismic tectonic loading, earthquake associated signals (co- and post- seismic), a seasonal term associated with weather related crustal loading and gravity, as well as man made signals such as changes in hardware, or location of each site.

We identify and separate the different signals in the positional time series by an iterative process in which a motion coherent to the whole continuous GPS network is also estimated and removed, allowing a precise estimation of the features present in the time series.

Figure 1:

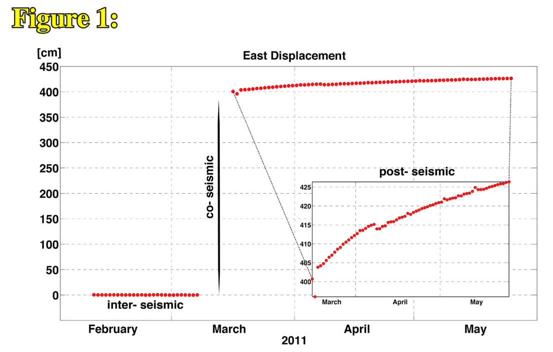

(a) Example of positional (daily) time series from continuous GPS in Japan. Signals from the 3 stages of the seismic cycle are labeled, where the co-seismic jump corresponds to the one of the 11 March 2011, Tohoku-Oki earthquake. The inset shows the post-seismic motion induced by such event as well as signals from several aftershocks.

$$
\begin{aligned}
u(t) &= u_0 + v\cdot t + \sum_i \left[EQco_i(t) + EQpos_i(t)\right] \\
&\quad + \sum_k \left[\beta^k H(t-t^k)\right] + S(t)
\end{aligned}
$$

where

$$
\begin{aligned}
EQco_i(t) &= u_c^i H(t-t_0^i) \\
EQpos_i(t) &= \alpha_R^i log\left(1+\frac{(t-t_0^i)}{\tau}H(t-t_0^i)\right) \\
HW_i(t) &= \beta^k H(t-t^k) \\
S(t) &= \left\langle sin\left(\frac{t}{T_1}+\phi_1\right), sin\left(\frac{t}{T_2}+\phi_2\right)\right\rangle
\end{aligned}
$$

(b) Model used to separate the signals present in the positional time series. A weighted least squares fit is performed to obtain the contribution of each signal in the positional data. Note that the earthquake and hardware changes times are assumed to be known, so careful inspection of all time series is required.

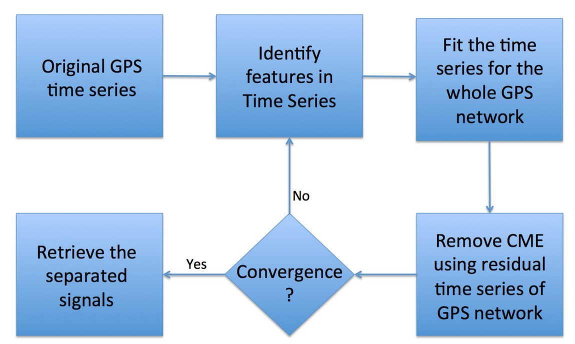

(c) Diagram describing the iterative process used to identify and separate the different features present in the positional time series, while

Figure 2:

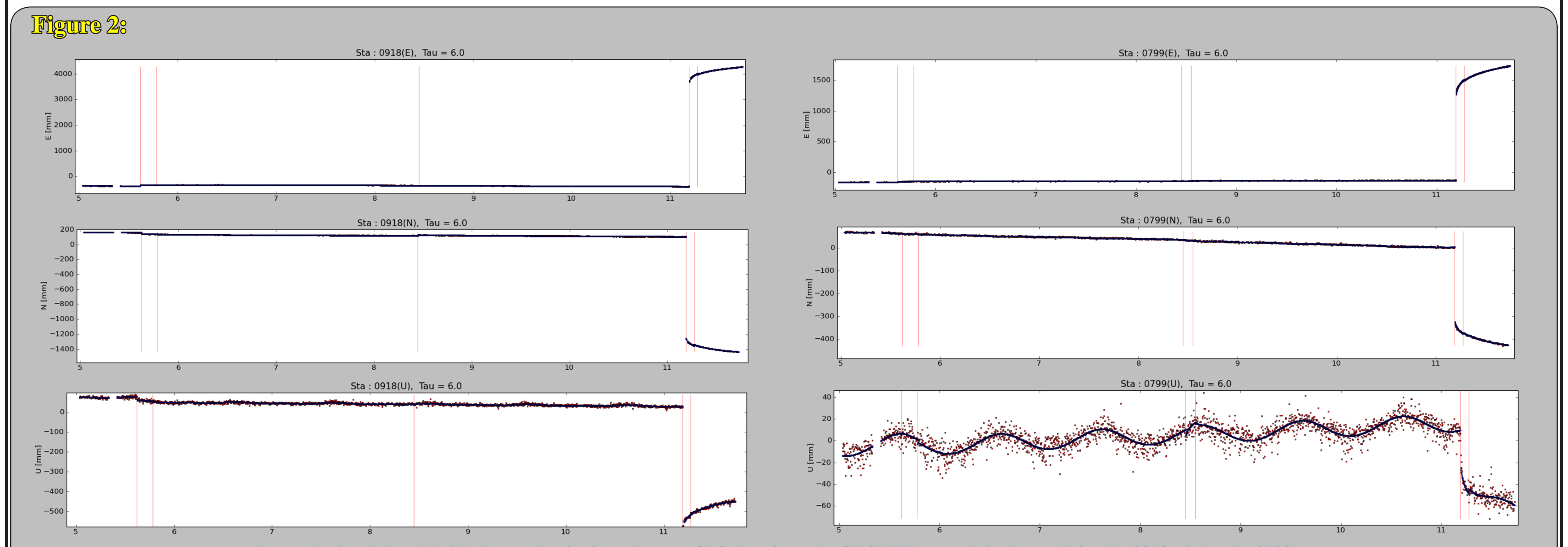

Example of positional (daily) time series for 2 continuous GPS sites from the GEONET network in Japan (left : site 0918, right: site 0799). Note the change of sign between co- and post-seismic vertical displacements for site 0918 as well as how noticeable is the seasonal signal in the vertical position of site 0799. We use the GEONET time series to estimate the co- and post- seismic displacements associated to the Tohoku-Oki earthquake.

Figure 3:

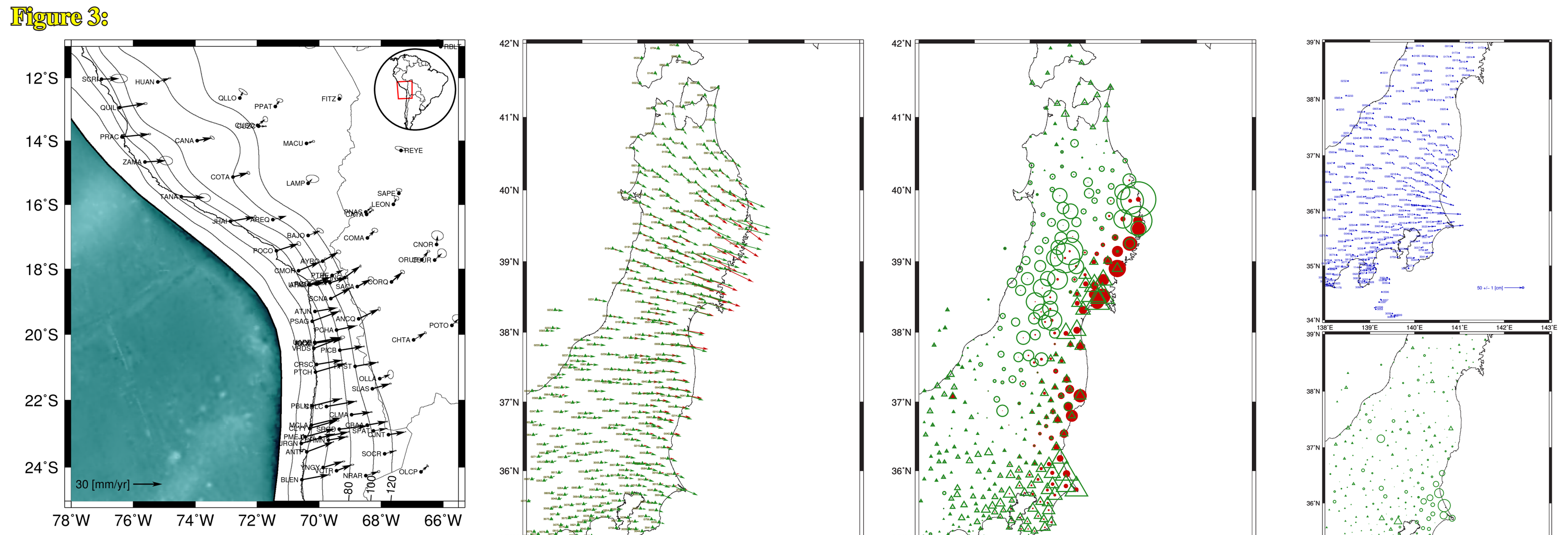

(a) Secular rates inferred from GPS observations for the Central Andes. Dataset consists of preciously published horizontal velocities from campaign GPS (Kendrick et al[2001, 2006]) as well as 3 component velocities from a recently stablished continuous GPS network in a collaborative effort of scientists from Chile, France, Perú and United States as a part of the Central Andes Tectonic Observatory (CAnTO).

(b) Co- and Post- seismic displacements associated to the 11 March 2011 (M9.0) Tohoku-Oki earthquake. Post-seismic displacements are estimated up to Sep 23, 2011. Note the change in direction of the horizontal post-seismic displacement with respect the co-seismic in northern Honshu, as well as the hinge line change from off-shore for the Mainshock to inland for the Post-seismic displacements.

(c) Horizontal and vertical co-seismic displacements for the Mw7.9 aftershock from 1Hz high rate cGPS data.

A Bayesian Approach to Estimating Apparent Plate Coupling
The Central Andean Subduction Zone

We paramterize the coupling along a 3D model of the plate interface by two interpolated curves at depth, defining a mask in which the plate interface is coupled in the region enclosed by these curves (yellow area) and uncoupled outside it.

Figure 4:

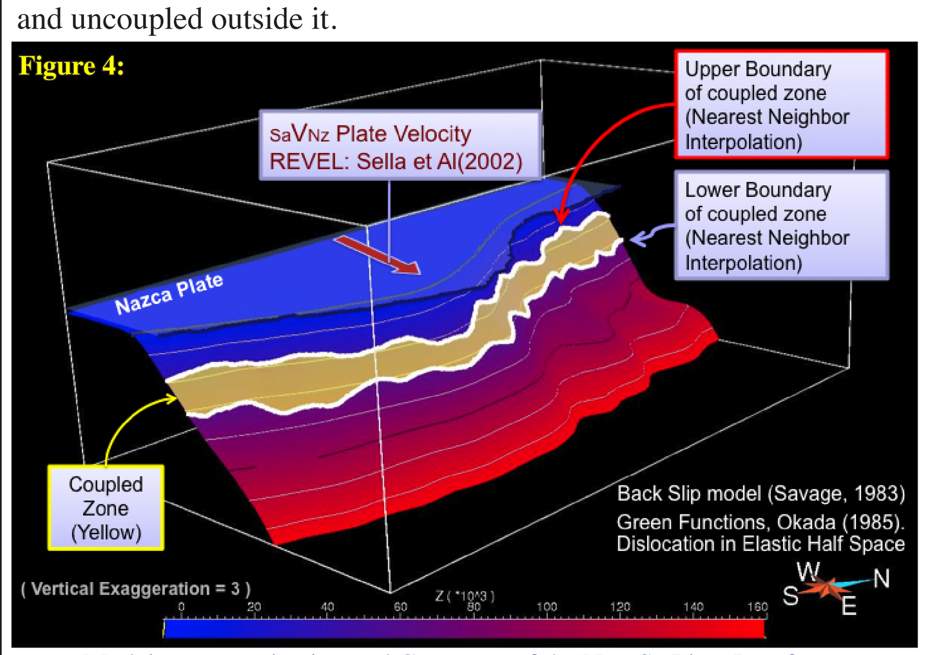

Model parameterization and Geometry of the Nz - Sa Plate Interface.

We use a back-slip model (Savage, 1983) to represent the inter-seismic strain accumulation at the plate interface, where a constant back-slip rate is imposed at the coupled zone. We ignore the possible existence of any transition zones. Plate convergence is represented by motion of a rigid plate on the sphere (Cox and Hart, 1986), with an Euler vector taken from the REVEL model (Sella et al, 2002). A finite dislocation in an elastic half space (Okada, 1985) is used to generate Green's functions. The geometry of the plate interface is built using GOCAD Suite, constrained with independent sets of geophysical data.

Free parameters of our model are the depth of the interpolation knots defining the updip and downdip boundary curves as well as a reference frame correction for each independent dataset (interseismic velocity field). Nearest neighbor interpolation is used in order to preserve the statistical properties of the knots depth for any interpolated point of the curve. Our Bayesian approach has no regularization other than the spatial scale imposed by the knot spacing.

We implement a Markov Chain Monte Carlo, Metropolis-Hastings (1970) algorithm for the inversion. The algorithm samples the *a posteriori* probability density function of the model: the depth of the k-th knot of the curves $Z_{upper\ boundary}(x)$ and $Z_{lower\ boundary}(x)$ defining the coupling at the plate interface.

Preliminary results: Coupling Probabilities

Figure 5:

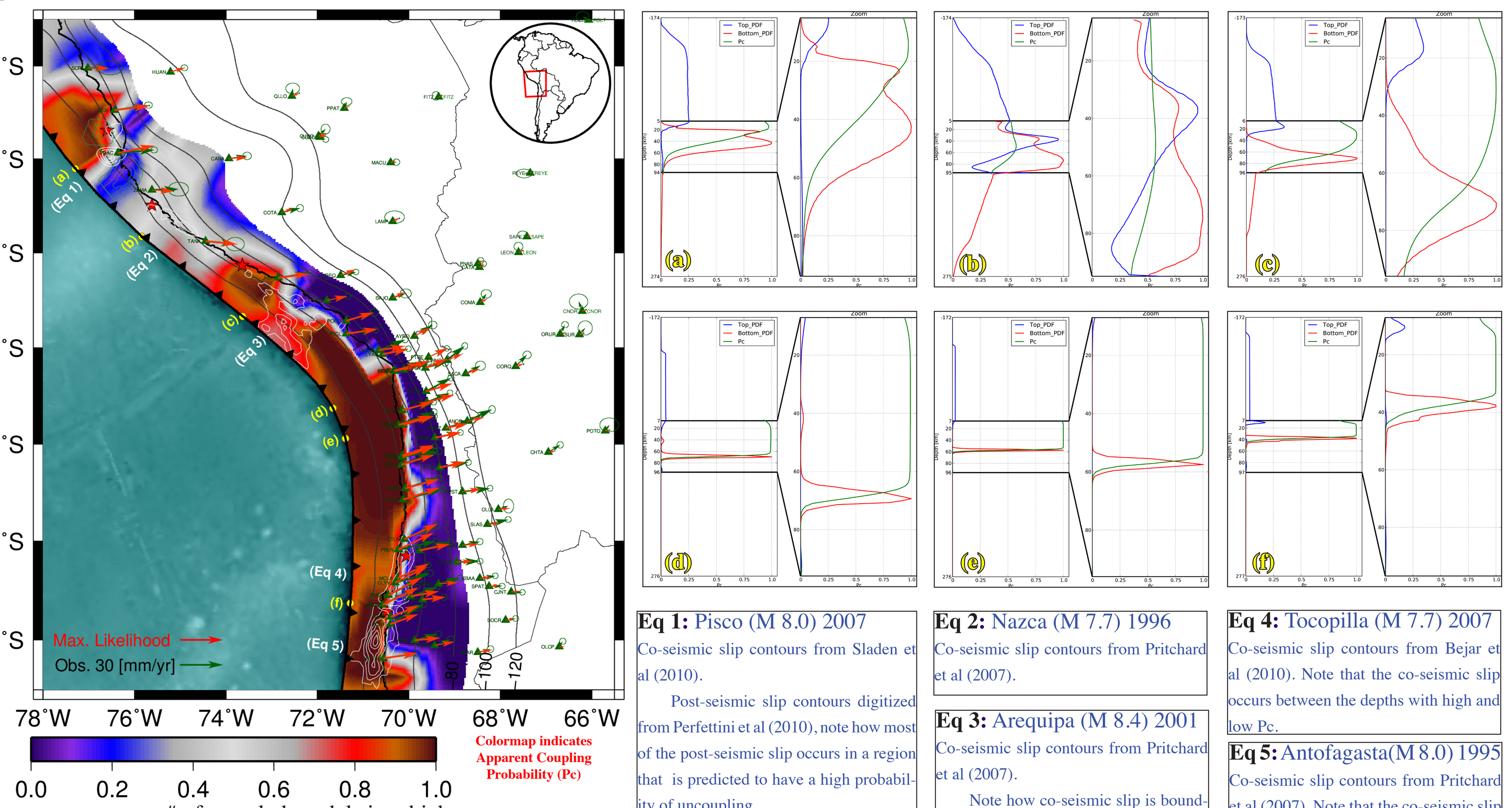

$$Pc(\mathcal{P}) = \frac{\#\ \text{of sampled models in which point}\ \mathcal{P}\ \text{is coupled}}{\#\ \text{of sampled models}}$$

Eq 1: Pisco (M 8.0) 2007
Co-seismic slip contours from Sladen et al (2010).
Post-seismic slip contours digitized from Perfettini et al (2010), note how most of the post-seismic slip occurs in a region that is predicted to have a high probability of uncoupling.
Note also how co-seismic slip and regions with high Pc are anticorrelated.

Eq 2: Nazca (M 7.7) 1996
Co-seismic slip contours from Pritchard et al (2007).

Eq 3: Arequipa (M 8.4) 2001
Co-seismic slip contours from Pritchard et al (2007).
Note how co-seismic slip is bounded (along strike) by 2 regions of high Pc and how these regions seems to be complimentary

Eq 4: Tocopilla (M 7.7) 2007
Co-seismic slip contours from Bejar et al (2010). Note that the co-seismic slip occurs between the depths with high and low Pc.

Eq 5: Antofagasta (M 8.0) 1995
Co-seismic slip contours from Pritchard et al (2007). Note that the co-seismic slip region is smaller than the region with high Pc in which the earhquake rupture occurs.

Our estimates of the a posteriori Pc constrained by the GPS velocities (green arrows) along with GPS velocity predictions of the maximum likelihood model (red arrows). Yellow dots and letters at the trench indicate perpendicular sections shown in side boxes, where Ztop, Zbottom PDFs and Pc are plotted for each section. White contours indicate co-seismic slip of past subduction earthquakes and green contours indicate Postseismic slip for Pisco M8.0 2007 earthquake from Perfettini et al 2010.

Concerns with current modeling and future validation

Figure 6:

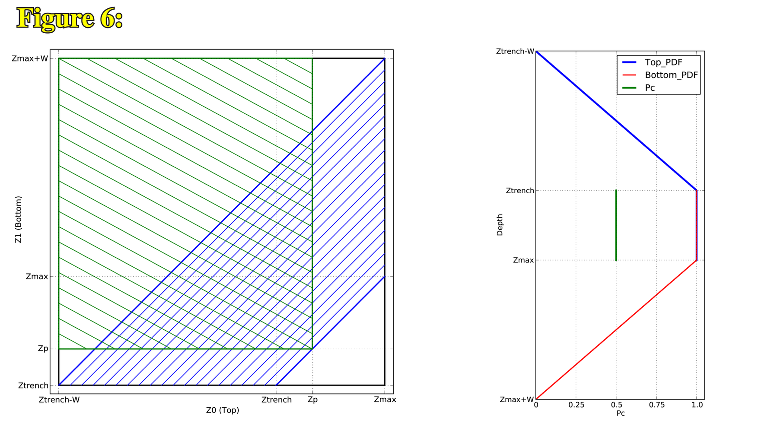

$$
\begin{aligned}
Z_{Top} &\approx U\left[Z_{trench}-W, Z_{max}\right] \\
Z_{Bottom} &\approx U\left[Z_{trench}, Z_{max}+W\right] \\
0 &\leq Z_{Bottom}-Z_{Top} \leq W \\
P_C = 0.5 &\Rightarrow W = 2\cdot(Z_{max}-Z_{trench})
\end{aligned}
$$

Our choice of a-priori restrictions, which produces Pc = 0.5 and uninformative (constant) PDFs for Ztop and Zbottom in the depth interval [Ztrench, Zmax]. Note that by definition Pc = 0 outside such interval.

The current coupling parameterization imposes that the coupled part of the plate must lie between 2 boundaries, therefore imposing a strong correlation between the location of such boundaries.

Due to a lack of off-shore observations, we have a strong constraint on the deep limit of the coupled region and a loose one on the shallow one. However, we obtain a high probability of coupling up to trench depth. Now we ask whether the observations are constraining the upper limit or it is just a result of our a-priori restrictions (Fig 6).

Further research is needed to validate the current results. To do so, we are going to adopt 2 approaches:

1) Compare our current results with the obtained by using slip inversion wise parameterization.

2) Use statistical indices as: the Kullback-Liebler divergence to show how different are the a priori and a posteriori PDFs of the model parameters; the mutual information between the all the a priori and a posteriori PDFs to measure how the dependence between the model parameters has been changed by the observational constraints.

Analysis of the Post-Seismic Deformation of the Great 11 March 2011 Tohoku-Oki (M9.0) Earthquake

Figure 6:

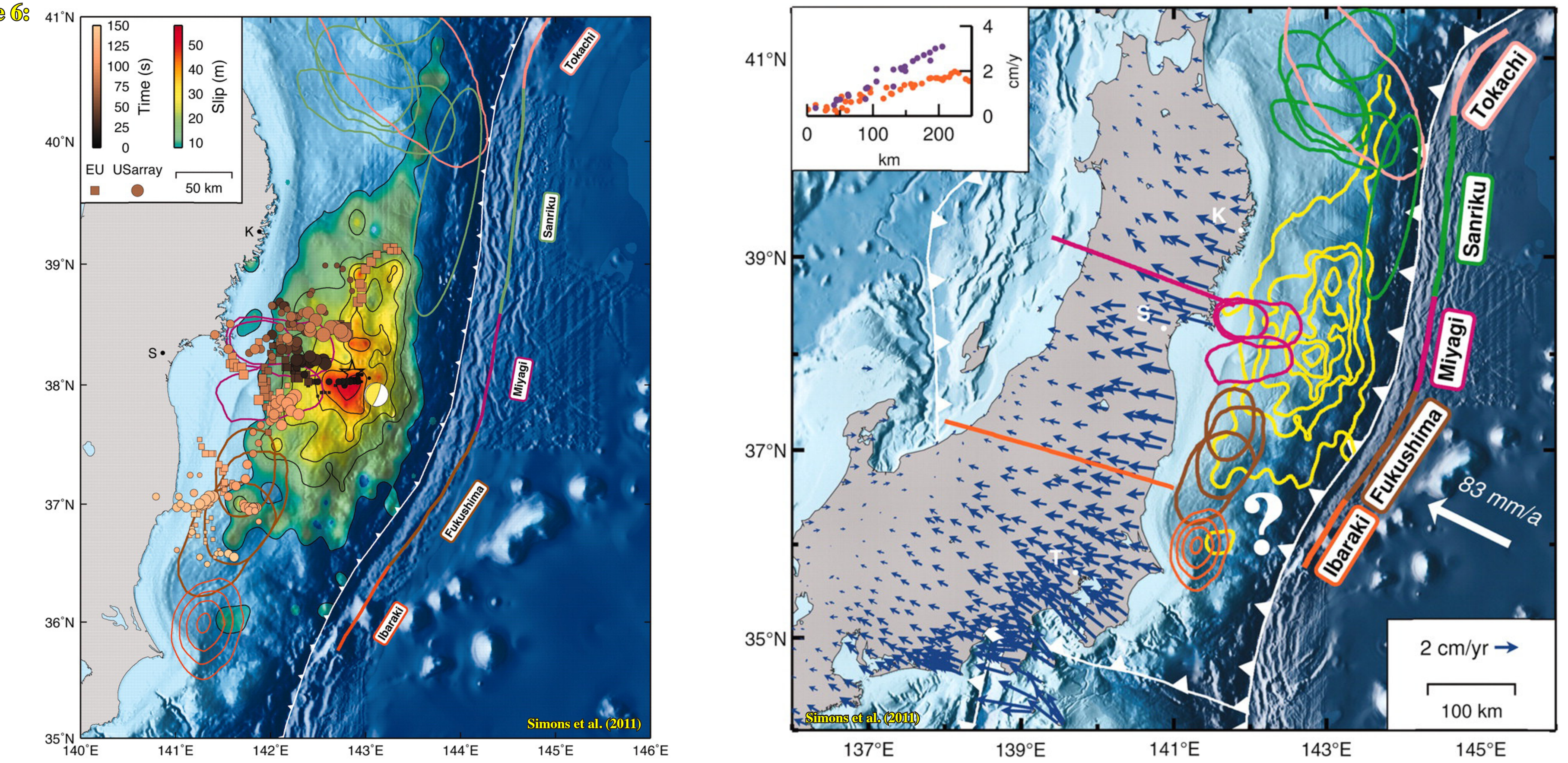

(a) Inferred distribution of subsurface fault slip (color and black contours with a contour interval of 8 m). Fault slip associated with the Mw 7.9 aftershock is indicated by nested 1-m orange contours. Approximate locations of historical megathrust earthquakes are indicated by closed curves colored by region: pink, Tokachi (1968 M8.2); green, Sanriku (1896 M8.5, 1901 M7.4, 1931 M7.6, 1933 M7.6); purple, Miyagi (1897 M7.4, 1936 M7.4, 1978 M7.4, 2005 M7.2); brown, Fukushima (1938 Mw 7.4, 1938 Mw 7.7, 1938 Mw 7.8). Location of points of HF radiation estimated using back-projection methods with data from the European Union seismic array and the USArray are indicated by squares and circles, respectively, with color intensity indicating time of the activity relative to the beginning of the event and with symbol size proportional to amplitude of the HF radiation normalized to the peak value. The star indicates the location of the Japan Meteorological Agency epicenter.

(b) Secular interseismic surface deformation (blue vectors) as observed by the GEONET continuous GPS network using the GSI F2 solution. The upper left inset shows the decrease of this deformation field at the latitude of the Miyagi (purple profile) and Ibaraki (orange profile) segments, with distance measured along the profile. The coseismic slip distribution is indicated by the yellow contours at 8-m intervals. The inset uses vectors within 100 km of the profile location. The question mark indicates a region of possible high seismic hazard.

Preliminary results: Least Squares Inversion of GPS data

Figure 7:

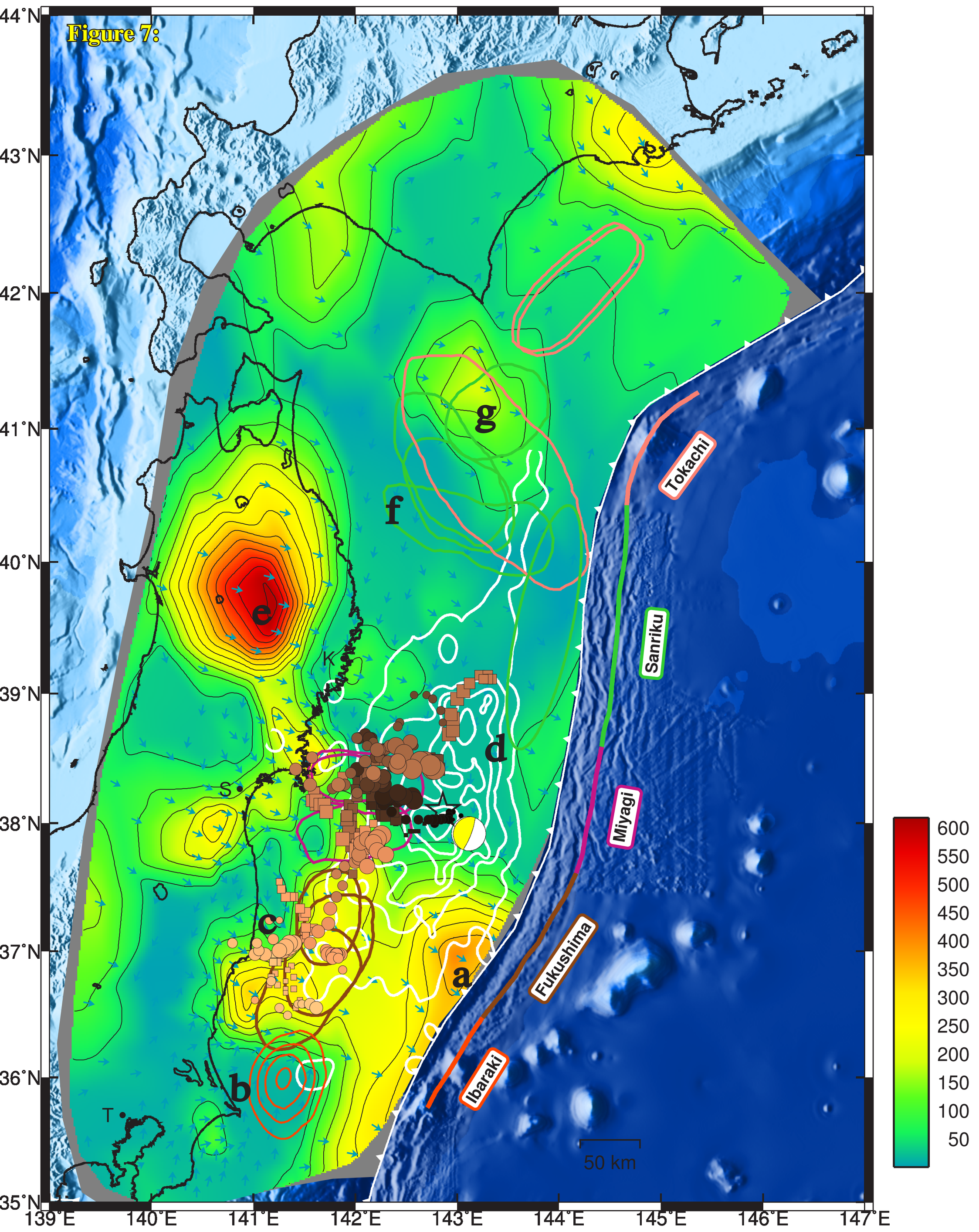

Our estimates of the Post-seismic slip associated to the M9.0 Tohoku-Oki earthquake. We performed a weighted least squares inversion with laplacian damping constrained by post-seismic crustal displacements measured from GPS data (Fig 3b) from Mainshock time up to 23 September 2011. Post-seismic slip contours are marked every 50 cm. White contours indicate the Tohoku-Oki mainshock slip distribution (8 meters contours). The 1m red contours represent the slip distribution of the M7.9 aftershock. Letters are explained in the right panel.

(a) Area with the "?" mark in Figure 6b, signaled as a region of possible high seismic risk just after the Tohoku-Oki earthquake (Simons et al, 2011). Our preliminary model infers high post-seismic slip (> 250 cm) in that area. But further research is needed in order to validate the high post-seismic slip close to the trench.

(b) Our model predicts zero post-seismic slip where the rupture process of the M7.9 aftershock occurs.

(c) Note how the location of points of High Frecuency radiation follows the boundary between 2 regions of low and high post-seismic slip. This is consistent with the hypothesis that the HF radiation may occur at the transition between brittle and ductile regions.

(d) The Tohoku-Oki rupture area with higher moment release has negligible post-seismic displacements.

(e) Region of high (> 6m in 6 months) post-seismic slip located below 100km depth. This patch of post-seismic slip is located just below the hinge line of vertical interseismic deformation. (Aoki and Scholz, 2002). The high post-seismic slip in this region suggest that it may remain locked (at least partially) interseismically and release the accumulated energy in episodes of aseismic slip.

(f) This region, predicted to hace negligible post-seismic slip, is also a region shown to have a small plate coupling in all the different published works. Thus suggesting that this area may be creeping constantly at a ratio close to plate convergence.

(g) This patch of post-seismic slip coincides with the estimated rupture area of the 1 968 (M8.2) Tokachi-Oki earthquake as well as with the southern patch of post-seismic deformation from the 2003 (M8.0) Tokachi-Oki earthquake.